Continuous-Phase Control of a Powered Knee-Ankle Prosthesis: Amputee Experiments Across Speeds and Inclines

David Quintero[1,2] **[Student Member, IEEE]**, **Dario J. Villarreal**[3] **[Student Member, IEEE]**, **Daniel J. Lambert**[4] **[Student Member, IEEE]**, **Susan Kapp**[5], and **Robert D. Gregg**[1,2] **[Senior Member, IEEE]**

[1]Department of Bioengineering, University of Texas at Dallas, Richardson, TX 75080 USA

[2]Department of Mechanical Engineering, University of Texas at Dallas, Richardson, TX 75080 USA

[3]Department of Electrical Engineering, Southern Methodist University, Dallas, TX 75275 USA

[4]Department of Electrical and Computer Engineering, University of Texas at Dallas, Richardson, TX 75080 USA

[5]Department of Rehabilitation Medicine, University of Washington, Seattle, WA 98104 USA

Abstract

Control systems for powered prosthetic legs typically divide the gait cycle into several periods with distinct controllers, resulting in dozens of control parameters that must be tuned across users and activities. To address this challenge, this paper presents a control approach that unifies the gait cycle of a powered knee-ankle prosthesis using a continuous, user-synchronized sense of phase. Virtual constraints characterize the desired periodic joint trajectories as functions of a phase variable across the entire stride. The phase variable is computed from residual thigh motion, giving the amputee control over the timing of the prosthetic joint patterns. This continuous sense of phase enabled three transfemoral amputee subjects to walk at speeds from 0.67 to 1.21 m/s and slopes from −2.5 to +9.0 deg. Virtual constraints based on task-specific kinematics facilitated normative adjustments in joint work across walking speeds. A fixed set of control gains generalized across these activities and users, which minimized the configuration time of the prosthesis.

I. INTRODUCTION

The vast majority of lower-limb amputees use mechanically passive prosthetic legs, which can only dissipate energy during locomotion. This limits an amputee's ability to efficiently perform various ambulation modes, such as walking at variable speeds or slopes. Furthermore, the biomechanical compensations required to walk with these passive devices generally cause joint discomfort and back pain during daily usage [1]–[3]. Powered prosthetic legs that provide actuation at the joints could potentially improve amputee gait.

Contact rgregg@ieee.org for further questions about this work.

Powered prostheses, especially those with multiple actuated joints, require sophisticated control strategies to perform various activities in a natural and safe manner [4]. The study of biomechanics classifies human gait into specific intervals over the gait stride, e.g., heel strike, pushoff, etc. [5]. Generally, powered prostheses mimic this ideology by using a different controller for each period of gait based on predefined transition criteria [6]. For example, finite state machines are commonly implemented with different joint impedance controllers for each discrete state/period [7]–[12]. However, the Proportional-Derivative (PD) gains and switching rules for each period must be carefully tuned for each user and activity. The configuration process for a powered knee-ankle prosthesis capable of navigating ramps [9] and stairs [13] can last several hours with a team of expert researchers [14]. Methods using offline (model-based) optimization [15], online optimization [16], [17], and rule-based online adaptation [18] have been proposed for automatically tuning these systems but are currently limited to a single actuated joint. Finite state machines based on quasi-stiffness and minimum-jerk swing trajectories are less sensitive to the user and walking speed [19], but sensitivity to other tasks remains an open question. Finite state machines can also end up in the wrong state after a perturbation, resulting in unexpected leg behavior that can lead to a fall.

To address these challenges, we propose a control method that unifies the different periods of gait through virtual kinematic constraints parameterized by a human-inspired phase variable and enforced by a torque control scheme. Often used to control bipedal robots [20]–[28], virtual constraints define desired joint trajectories as functions of a monotonically increasing mechanical signal called a phase variable. A phase variable corresponds to an unactuated degree of freedom that increases (or decreases) relative to the forward (or backward) progress through a rhythmic process [20]. The proposed controller enslaves prosthetic joint patterns to the progression of a phase variable under the control of the amputee's hip.

The choice of phase variable makes a difference in how the prosthetic leg responds to the user's movement or the environment. A recent study found that the thigh phase angle robustly represents the timing of distal joint patterns during non-steady walking [29], [30]. This provides a human-inspired phase variable that could allow a prosthetic knee and ankle to remain in synchrony with the user across changes in walking speed or the environment. Directly controlling prosthetic joints through the user's hip motion could also encourage a stronger embodiment of the prosthesis [31]. The proposed control strategy continuously parameterizes the gait cycle by measuring this phase variable from a single inertial measurement unit (IMU) mounted above the prosthetic knee joint.

Previous work in phase-based control of wearable robots has been limited to piecewise unification of the gait cycle or single-joint control rather than coordinated control of multi-joint kinematics. The virtual constraint approach was used in [32] to unify the stance period of a powered knee-ankle prosthesis, but the swing period was still divided into a state machine. The stance and swing periods were separately unified in [33], [34] and subsequently in [35], but switching between these two periods can cause undesirable delays and discontinuities. The powered ankle prosthesis in [36] is controlled in a unified manner by the tibia phase angle, which is not as well correlated with a phase oscillator as the thigh

phase angle [29]. The hip exoskeletons in [37], [38] use the hip angle to drive the dynamics of an artificial phase oscillator that determines when to inject or dissipate energy, which may not be sufficient to replicate joint kinematics in a prosthesis application. In our work, virtual constraints produce the desired kinematics in the absence of biological limb motion. Both [36] and [37] use angular velocity in the computation of the phase angle, which presents a few challenges for real-time control such as sensitivity to noise from impacts. Angular velocity also makes the phase variable only one derivative away from the equations of motion, i.e., relative degree-one [39], which prevents the use of derivative error corrections in the controller [30]. In this paper we utilize a relative degree-two version of the thigh phase angle based on angular position and its integral.

We parameterize periodic virtual constraints with the thigh phase angle in order to continuously define the desired joint kinematics across strides. In particular, virtual constraints defined with the Discrete Fourier Transform (DFT) encapsulate the property of periodicity [40], which respects the repetitive nature of the gait cycle. The conceptual design of DFT virtual constraints was studied in simulations of an amputee biped model in [40], demonstrating that the continuous-phase controller can produce stable walking for various walking speeds. Preliminary experiments with this control method were conducted with an able-bodied subject wearing a powered knee-ankle prosthesis through a leg bypass adapter in [41].

The primary contributions of this paper are 1) extending the continuous-phase control approach to different walking speeds and ground slopes, 2) determining the importance of task-specific kinematics in the virtual constraints, and 3) demonstrating that the parameters of this control approach generalize across multiple amputee subjects. Periodic virtual constraints are designed for different speed and slope conditions based on able-bodied human data. Using a custom powered knee-ankle prosthesis, three transfemoral amputee subjects were able to walk naturally at speeds from 0.67 to 1.21 meters/sec and ground slopes from −2.5 to +9.0 degrees (deg) using the same control parameters. The phase variable provided temporal adaptation to different conditions, but task-specific kinematics in the virtual constraints were necessary for the prosthesis to appropriately adjust its mechanical work. Because the control parameters were insensitive to the user, the configuration time of the powered knee-ankle prosthesis was greatly reduced compared to state-of-art methods [4].

II. HARDWARE SETUP

This section describes the robotic prosthetic leg (Fig. 1) used to implement and test the control method.

A. Powered Prosthesis Actuation Design

A powered knee-and-ankle prosthesis was designed and built at the University of Texas at Dallas (UTD) as a research platform for testing control strategies. The design requirements were based on the joint kinematics and kinetics of able-bodied walking on level ground and inclines [5]. The range of motion is 0° to −70° at the knee joint and −20° to 25° at the ankle joint. The knee and ankle actuators were optimized for fast walking on level-ground,

resulting in a design that can achieve a maximum torque of 40 Nm and 120 Nm, respectively. The torque demand varies based on the weight of the subject, but this design is sufficient for a 75 kg user.

An electromechanical linear actuator with a lever arm at each joint (similar to [8]) was designed to meet the torque requirement while limiting weight. A high power-to-weight ratio Maxon EC-4pole 30, 200 Watt, three-phase Brushless DC (BLDC) Motor provides input power to the transmission. The motor output shaft is connected to a linear ball screw through a timing belt drive with 7075 aluminum sprockets (with a 2:1 reduction at the knee and 4:1 at the ankle). A Nook 12 mm diameter, 2 mm lead ball screw converts the sprocket's rotary motion into linear motion of the ball nut, which drives a lever arm to generate the joint torque. Although the resulting gear ratio depends on the joint angle, the average ratio is 360:1 at the knee and 720:1 at the ankle. Each ball screw is supported axially and radially by a Nook double bearing support journal. A motor mount with a rotational pivot was designed to eliminate buckling of the ball screw and increase its linear motion as it travels up/down to rotate the joint via the lever arm, providing the desired range of motion at each joint. Hard stops at the end of the ball nuts were 3D printed from a polyjet material to eliminate ball screw travel beyond its intended range. Fig. 1 displays key design components of the actuation system for the powered prosthesis. Overall, the mass of the leg is 4.8 kg, which is comparable with other powered knee-ankle legs in the literature [8]–[10], [42].

B. Embedded Systems and Sensing

Offboard computation and power is provided to the powered leg through a tether. A dSPACE DS1007 system with Freescale OorIQ P5020, dual-core, 2 GHz PowerPC processor provides real-time control and data acquisition at 1 kHz for this research platform. A 35V/60A DC power supply (Agilent Technologies, 6673A) provides power to the onboard motor amplifiers, and a separate DC power supply (BK Precision, 1761) provides power to the onboard sensors.

The sensors and motor drivers are located onboard the powered leg. For low-level control, each motor has an incremental, 3000 counts-per-turn quadrature encoder (Maxon, 2RMHF). The motors are driven by a motor amplifier (Copley Controls, ADP-090-36) using three-phase sinusoidal commutation for current control. An inductance filter card (Advanced Motion Controls, BFC10010) with 0.200 mH inductors per phase is embedded inline between the motor phase lines and the motor amplifier to increase the impedance load for the amplifier to operate the low-inductance BLDC motor (terminal inductance phase to phase at 0.0163 mH). In order for the rigid ankle actuator to achieve compliant and forceful interaction with the ground [11], [43], [44], a uniaxial force sensor (Futek, LCM200) is installed inline with the ankle's ball screw to provide feedback for a closed torque loop (Section III-B). This force sensor is connected to an offboard analog amplifier (Futek, CSG110). A force sensor could not be used in the knee actuator due to off-axis overloading during peak knee flexion.

For joint-level control, each joint has a high resolution, 4000 cycles-per-revolution optical encoder (US Digital, EC35) mounted to the joint's output shaft. Joint velocities are computed numerically with a first-order low-pass Butterworth filter at 8 Hz cutoff frequency.

Using a joint PD controller to track a position sine sweep, benchtop experiments determined that the closed-loop position bandwidth (defined by −3 dB magnitude crossover frequency) exceeds 3.5 Hz at each joint. This performance is sufficient for tracking human joint trajectories during walking (frequencies up to 2 Hz) [5], [10].

In order to compute the phase variable in Section III-A2, an IMU (LORD MicroStrain, 3DM-GX4-25) is mounted above the prosthetic knee in the sagittal plane. The IMU contains a triaxial accelerometer, gyroscope, and magnetometer. Dual on-board processors run an Adaptive Kalman Filter based on Newton's and Euler's equations of motion to compute real-time Euler Angles in the IMU coordinate frame at a sampling rate of 500 Hz. Velocities of the Euler angles are estimated with a low-pass filter to reduce sensor noise as in [45].

III. CONTROL METHOD

This section presents the control scheme implemented on the powered knee-ankle prosthesis. The outer loop performs high-level joint position control to enforce periodic virtual constraints parameterized by a human-inspired phase variable. We then describe an inner loop that performs low-level torque control based on torque commands from the outer loop controller. These two control loops are depicted in Fig. 2.

A. Outer Control Loop

The outer loop controller coordinates the knee and ankle patterns of the prosthetic leg by enforcing virtual constraints based on a common phase variable. Virtual constraints encode the desired motions of actuated variables in output functions to be zeroed through the control action [20]:

$$y_i = q_i - h_i^d(s_h), \quad (1)$$

where q_i is the measured angular position of joint i (with $i = k$ for the knee or $i = a$ for the ankle), and h_i^d is the desired joint angle trajectory as a function of the normalized phase variable $s_h \in [0, 1)$. We will design h_k^d and h_a^d in Section III-A1 and s_h in Section III-A2 for application to the powered prosthesis.

Eq. 1 is considered the tracking error of the control system. Various torque control methods can be utilized to regulate this error. Bipedal robots typically enforce virtual constraints using input-output feedback linearization [20]–[26], which has appealing theoretical properties including exponential convergence [39], reduced-order stability analysis [20], and robustness to model errors [22]. However, to apply feedback linearization to a prosthesis, the dynamics of the prosthesis and the interaction forces with the human user and ground must be known [32], [33]. Identifying a sufficiently accurate model of the prosthetic leg is difficult, and measuring interaction forces requires expensive multi-axis load cells. Therefore, we utilize a model-free torque control method in this application, specifically output PD control [32], [40].

Output PD controllers typically have the form

$$\tau_{di} = -K_{\mathrm{p}i}y_i - K_{\mathrm{d}i}\dot{y}_i, \quad (2)$$

where $K_{\mathrm{p}i} > 0$ is the proportional gain affecting the stiffness of joint i about its angular trajectory, and $K_{\mathrm{d}i} > 0$ is the derivative gain correcting velocity tracking error $\dot{y}_i$. Controlling both the position and velocity of the output is helpful for tracking the desired trajectories but can create forceful interaction with the human user. More compliant, smooth behavior can be achieved by replacing $\dot{y}_i$ with the measured angular velocity $\dot{q}_i$ in Eq. 2. This was done in the knee controller for user comfort, but the ankle controller was left in the form of Eq. 2. This PD control method determines the joint torques needed to enforce the virtual constraints.

1) Periodic Virtual Constraints—Virtual constraints are time-invariant relationships between coordinates, where a monotonic, unactuated coordinate called a phase variable serves the role of time [20]. If the phase variable is monotonic over a complete gait cycle (as designed in Section III-A2), then it is possible to parameterize a periodic joint trajectory with a single output function. The DFT will be used to obtain such a function from able-bodied human data.

Consider a desired joint trajectory expressed as a function of some monotonically increasing quantity. Let the discrete signal $x[n]$ represent this trajectory sampled over N evenly distributed points. The DFT is a linear transformation of the signal $x[n]$ that produces a sequence of complex numbers across a spectrum of discrete frequency components $X[k]$:

$$X[k] = \sum_{n=0}^{N-1} x[n]W_N^{kn}, \quad k = 0, 1, \ldots, K, \quad (3)$$

where N is the finite number of samples, k is the running index for the finite sequence of K $\leq N-1$ frequency components, and $W_N = e^{-j(2\pi/N)}$ is the complex quantity [46]. Because the time-domain signal $x[n]$ is periodic, there are a finite number of discrete frequencies $X[k]$.

After obtaining the frequency components $X[k]$, the original signal can be reconstructed using Fourier Interpolation:

$$x[n] = \frac{1}{N}\sum_{k=0}^{K} X[k]W_N^{-kn}, n = 0, 1, \ldots, N-1, \quad (4)$$

where $X[k] = \mathrm{Re}\{X[k]\} + j\,\mathrm{Im}\{X[k]\}$ and $W_N^{-kn} = \mathrm{Re}\{W_N^{-kn}\} + j\mathrm{Im}\{W_N^{-kn}\}$ in standard complex form. Since the joint kinematic signals are real numbers, only the real part of $x[n]$ remains in Eq. 4 (see [46]). Eq. 4 can then be decomposed as a summation of sinusoids

using Euler's formula $e^{\pm j\Omega} = \cos\Omega \pm j\sin\Omega$ for $\Omega \in \mathbb{R}$ in W_N. From this we can obtain the desired joint angle as a function of a normalized phase variable $s_h \in [0; 1)$:

$$h^d(s_h) = \frac{1}{2}\rho_0 + \frac{1}{2}\rho_{\frac{N}{2}}\cos(\pi N s_h) + \sum_{k=1}^{\frac{N}{2}-1}\left[\rho_k\cos(\Omega_k s_h) - \psi_k\sin(\Omega_k s_h)\right], \quad (5)$$

where $\Omega_k = 2\pi k$, and ρ_k and ψ_k are the computed coefficients from the real and imaginary terms of $X[k]$ in Eq. 4. Because Eq. 5 is composed of sine and cosine functions, the resulting output function (Eq. 1) is bounded and inherently periodic across the normalized phase variable with a period of one.

Given desired knee and ankle trajectories over the gait cycle, Eq. 5 defines the periodic virtual constraints for the powered prosthesis. Different sets of virtual constraints were generated for a variety of speed and slope conditions, specifically level-ground walking at slow, normal, and fast speeds using averaged able-bodied human data from [5] and normal-speed walking on ground slopes of −2.5, 2.5, 5.0, 7.5, and 9.0 deg using averaged able-bodied data from [47]. These virtual constraints were parameterized by the normalized version of the phase variable ϑ from Section III-A2, i.e.,

$$sh(\vartheta) = \frac{\vartheta - \vartheta^+}{\vartheta^- - \vartheta^+}, \quad (6)$$

where '+' and '−' indicate the starting value of the prosthetic stance period and the ending value of the prosthetic swing period, respectively.

2) Human-Inspired Phase Variable—Our choice of phase variable is motivated by a study [29] showing that the thigh phase angle robustly parameterizes ipsilateral leg joint patterns during non-steady human walking, e.g., across perturbations. This choice of phase variable also has connections to biology, as hip motion is known to be a major contributor to synchronizing the leg joint patterns in mammals [48]. The thigh angle is measured with respect to the vertical gravity vector (i.e., a global angle) by the previously described IMU.

Although the thigh phase angle can be easily computed offline from post-processed kinematic data [29], real-time computation presents a challenge for implementation in a prosthetic control system. In particular, the phase angle is typically computed from the angular position and velocity [36], [37], but angular velocity is prone to noise and makes the control system relative degree-one [30]. We instead compute a phase angle $\vartheta(t)$ utilizing thigh angular position $\phi(t)$ and its integral $\Phi(t) = \int_0^t \phi(\tau)d\tau$ in the following way:

$$\vartheta(t) = \text{atan2}((\Phi(t) + \Gamma)z, (\phi(t) + \gamma)), \quad (7)$$

where the scale factor z, the thigh angle shift γ, and the thigh integral shift Γ are given by

$$z = \frac{|\phi_{max} - \phi_{min}|}{|\Phi_{max} - \Phi_{min}|},$$

$$\gamma = -\left(\frac{\phi_{max} + \phi_{min}}{2}\right), \quad \Gamma = -\left(\frac{\Phi_{max} + \Phi_{min}}{2}\right).$$

These parameters center the thigh orbit around the origin and maintain an approximately constant orbital radius, which improves the linearity of the phase variable trajectory.

The integral is reset every gait cycle to prevent the accumulation of drift due to variation in thigh kinematics. The scale and shift parameters are recalculated every quarter gait cycle, i.e., at each axis crossing in the phase portrait. Because these updates occur when the phase angle radius is collinear with the axis, the phase angle calculation (Eq. 7) remains continuous. Fig. 3 shows the scaled/shifted orbit in the thigh phase plane over several strides, where changes in circular orbit diameter are associated with changes in walking speed. Finally, the phase angle from Eq. 7 is normalized according to Eq. 6 with constants $\vartheta^+ = 0$ and $\vartheta^- = 2\pi$.

B. Inner Control Loop

The torque commands of the outer loop (Section III-A) are converted into current commands for the BLDC motor drivers in two ways. The desired input current to the knee motor is determined by dividing the desired knee torque by the motor's torque constant (0.0136 Nm/A) and the estimated gear ratio between the motor and joint. To provide compliant and forceful interaction with the ground, the ankle torque command is enforced by a closed torque loop (the inner loop in Fig. 2). The torque loop compensates for the actuator dynamics and external loads to reduce torque tracking error. The torque loop has two parts: a Proportional-Integral (PI) controller based on torque feedback and a friction compensator to reduce the effects of the ball screw transmission.

The friction compensator is defined as a function of ankle joint velocity:

$$u_a^F(t) = (F_C + F_v|\dot{q}_a(t)|)\text{sgn}(\dot{q}_a(t)), \quad (8)$$

where $F_C = 0.3$ is the Coulomb friction coefficient and $F_v = 0.01$ is the viscous friction coefficient of the ankle actuator. The torque PI controller is given by

$$u_a^\tau(t) = -K_p^\tau e_a(t) - K_I^\tau \int_0^t e_a(\sigma)\,d\sigma, \quad (9)$$

where $e_a = \tau_{\mathrm{m}a} - \tau_{\mathrm{d}a}$ is the ankle torque error between the measured torque $\tau_{\mathrm{m}a}$ and the desired torque $\tau_{\mathrm{d}a}$. The measured torque $\tau_{\mathrm{m}a}$ is determined by the ball screw linear force F_l and the angle of attack of the ball screw to the lever arm from the ankle joint forward kinematics (see Fig. 2). The torque proportional gain K_{p}^{τ} compensates for the current values of the error, while the torque integral gain K_{I}^{τ} reduces the offset between the measured and desired torques as error accumulates over time. Finally, the desired motor current

$$u_a^A = u_a^F + u_a^{\tau} \quad (10)$$

is sent to the ankle motor amplifier, which runs an internal current loop.

IV. EXPERIMENTS

This section describes the experimental setup, protocol, and results with three amputee subjects walking at different speeds and inclines. The experimental protocol was approved by the Institutional Review Board (IRB) at the University of Texas at Dallas. Handrails and/or a safety harness were provided to prevent falls, though no adverse events occurred.

A. Initial Setup and Tuning

The control parameters used in the amputee experiments were determined through benchtop and able-bodied testing. First, the top of the prosthetic knee joint was mounted to a rigid bench. The control parameters in Section III were tuned while the joints tracked walking trajectories based on prerecorded phase variable measurements. After finding a set of control parameters that reasonably enforced the virtual constraints, the prosthesis was mounted onto a leg-bypass adapter that allows an able-bodied subject to walk on the prosthesis. The IMU was mounted above the prosthetic knee joint and aligned in the sagittal plane.

An able-bodied human subject walked on the powered prosthesis as in [41]. After recording several strides of IMU data, a Principal Component Analysis (PCA) was done to compute a transformation matrix that further decouples the Euler angles of the frontal and sagittal planes [49]. Control parameters were then re-tuned as the able-bodied subject walked on a level treadmill at their comfortable speed. The knee joint parameters were reduced to account for the aiding hip moment and to produce less forceful interaction with the user, resulting in slightly more knee angle tracking error. The ankle torque control parameters (Eq. 9) were increased to provide more push-off torque against the weight of the subject. The friction compensator parameters from Eq. 8 remained the same. The control parameters at the end of this tuning process ($K_{\mathrm{p}}^{\tau} = 1.0$, $K_{\mathrm{I}}^{\tau} = 1.0$, $K_{\mathrm{p}a} = 16.5$, $K_{\mathrm{d}a} = 1.5$, $K_{\mathrm{p}k} = 2$, $K_{\mathrm{d}k} = 0.12$) were used for all three amputee subjects.

B. Amputee Experiment Protocol

Experiments were conducted with three transfemoral amputee subjects (TF01–03) as reported in Table I. Each subject met the inclusion criteria, e.g., weight less than 113 kg, 18 to 70 years in age, and no neuromuscular disorder or secondary health problems that would

prohibit their ability to participate in the study activities. All subjects had zero to minimal experience using a powered prosthesis.

A certified prosthetist attached the powered prosthesis to each subject's current, well-fitting custom socket (Fig. 4) and aligned the prosthesis appropriately. The subjects became acclimated to the powered prosthesis by walking overground along handrails for about 20 minutes. The transformation matrix for decoupling the IMU Euler angles was also computed during this period. Once acclimated, the subject participated in treadmill experiments with different speeds and inclines. The same control gains were used across all trials.

The subject first walked on a level treadmill at different speeds with virtual constraints corresponding to slow, normal, or fast kinematics (Section III-A1). Walking speeds are reported in the units of the treadmill, miles per hour (mph). Initially, the subject walked as the treadmill speed incrementally increased to 2.0 mph (0.89 meters/sec) to verify that this was a comfortable, normal walking speed. Then, the slow and fast speeds were defined at 1.5 mph (0.67 meters/sec) and 2.5 mph (1.12 meters/sec), respectively. Individual slow, normal, and fast speed trials were performed at the subject's discretion with the corresponding kinematics for a minimum of 30 seconds to capture a consecutive sequence of steady-state strides. The subject was also given the option to walk at a very fast speed of 2.7 mph (1.21 meters/sec) with the fast kinematics. Trials were then performed at these speeds using fixed normal-speed kinematics to examine the adaptability provided by the phase variable alone.

Next, the subject walked at the normal speed on different treadmill inclines using the corresponding virtual constraints (Section III-A1). The subject started on a slope of −2.5 deg (the minimum slope of the treadmill). Then the slope was incremented by +2.5 deg until reaching the user's maximum comfortable slope or +9.0 deg (the maximum slope of the treadmill). Walking data was recorded at each slope condition for at least 15 seconds. The subjects also walked successfully on variable inclines using fixed joint kinematics, but those results are withheld in Section IV-C due to space limitations.

C. Amputee Results

The range of speeds and slopes achieved by each subject is given in Table II. A supplemental video of all subjects walking across these conditions is available for download. We first highlight results at the normal walking speed on level ground and then present differences over speeds and inclines.

1) Normal Level-Ground Walking—Fig. 5 shows the phase portraits of prosthetic joint angles vs. velocities for all three amputee subjects walking on level ground at 2.0 mph with the normal-speed virtual constraints. Each subject was able to walk comfortably with the prosthesis and achieve a normative periodic orbit over consecutive strides. The phase portrait of subject TF01 exhibits the least variance due to more consistent hip motion. However, slower hip motion during swing resulted in slower prosthetic knee extension for this subject.

Fig. 6 displays the prosthesis kinematics and kinetics for TF01 averaged over 20 consecutive strides. The phase variable exhibits a nearly linear, monotonically increasing trajectory over

time (Fig. 6i). The small variability about the mean can be attributed to normal within-stride variability between stance and swing, e.g., the phase variable exhibits a shallower slope during a longer stance period and a steeper slope during a shorter swing period. This behavior synchronized torque and power delivery with critical phases of the gait cycle (Fig. 6e–h) and resulted in consistent, smooth joint motion (Fig. 6a–d).

The commanded vs. measured joint angles are shown over normalized time in Fig. 6a–b and over the phase variable in Fig. 6c–d. Because virtual constraints define the desired joint angles as functions of the phase variable, the commanded position only exhibits variance over normalized time. This temporal variability is associated with temporal variability in the phase variable based on the user's progression within the gait cycle (Fig. 6i), which resulted in slower or faster progression through the desired prosthetic trajectories. The measured joint kinematics exhibit small variance over both time and phase variable, demonstrating consistency over multiple consecutive strides. Some phase delay can be observed between the measured and commanded signals, which can be attributed to the reflected inertia of the actuators and the lower control gains employed for user comfort.

Fig. 6e–h display the joint torques and powers over the phase variable, which more accurately captures the within-stride progression of the user [29]. The knee torque and power was smaller than normal during stance ($s_h \in [0, 0.6]$) because of the non-backdrivable actuator design, which can support the weight of the amputee without much input from the motor. During swing period ($s_h \in (0.6, 1.0]$), the knee joint provides appropriate torque and power to help flex and then extend the knee. The ankle torque and power follow the curved shape of able-bodied data, particularly giving push-off torque and power during late stance. The measured values are lower than able-bodied averages due to the small control gains.

Fig. 6j provides box plots of the normalized mechanical work (J/kg) per stride for each joint (i.e., the time-integral of normalized joint power (W/kg) per stride). The ankle did positive work over the stride, behaving as an energy generator and giving the positive power needed for push-off [43]. The knee joint did negative work due to the negative power required for normative swing biomechanics [50]. The total work done by the prosthesis was close to zero, demonstrating a normative energy balance between the two joints [5].

2) Variable Speeds—Fig. 7 shows the averaged results for TF02 walking at different speeds with *matched* kinematics. The slope of the temporal phase variable trajectory increased with walking speed (Fig. 7g) due to the faster motion of the user's hip. This resulted in faster progression through the prosthesis joint patterns to match the shorter stride period. The prosthesis provided appropriate kinematics by enforcing the different virtual constraints for slow, normal, and fast walking (Fig. 7a–b), where the joint range of motion increased for the faster kinematics. The subject also performed a very fast trial (2.7 mph) using the fast kinematics, and some dynamic adaptation can be seen compared to the fast trial (2.5 mph). For example, the prosthesis exhibited greater ankle dorsiflexion during early stance ($s_h \sim 0.2$) in the very fast trial.

Torque and power delivery (Fig. 7c–f) during stance increased at faster speeds as observed in able-bodied data [5]. This resulted in more (positive) ankle work and total work at faster

speeds (Fig. 7h), thus providing more assistance to the user. The subject spent more time in stance (i.e., a later stance-to-swing transition) while walking at the slow speed, resulting in some differences from the faster speeds. For example, the slow speed exhibited a longer period of ankle pushoff torque and power (with less magnitude). At the slow speed, the knee had a large peak of negative power during swing flexion ($s_h \sim 0.65$), possibly to slow the knee while the user's hip rapidly accelerated to complete the shorter swing period.

Subject TF02 was able to walk at the same range of speeds using *fixed normal-speed* kinematics (Fig. 8) due to the temporal adaptation provided by the phase variable. In particular, the phase variable exhibited speed-appropriate slopes over time (Fig. 8g), which appropriately slowed or accelerated the prosthetic leg's progression through its fixed joint trajectories. The different load conditions for slow and fast walking resulted in some dynamic adaptation in the prosthetic joint kinematics, especially at the slow speed (Fig. 8a–b). However, the fixed kinematics did not allow the joint kinetics (Fig. 8c–f) to adjust appropriately to changing speed. In particular, the ankle did not increase its torque and power output with walking speed as in the matched kinematics experiments (Fig. 7c–f). This resulted in a relatively flat trend in ankle work and total leg work as speed increased (Fig. 8h). These experiments demonstrate that fixed virtual constraints can provide adequate function at different walking speeds, but speed-matched virtual constraints promote more natural gait biomechanics, especially energetics.

3) Variable Inclines—Fig. 9 shows the averaged results for the different inclines (−2.5 deg to +9.0 deg) performed by TF02. Because the treadmill speed was consistent (2.0 mph) across inclines, the temporal phase variable trajectory remained consistent (Fig. 9g). The prosthesis provided appropriate kinematics by enforcing the different virtual constraints for each incline condition (Fig. 9a–b), where the knee joint (Fig. 9a) has more flexion from heel strike ($s_h \sim 0$) to heel rise ($s_h \sim 0.45$) at steeper inclines. The ankle joint (Fig. 9b) exhibited more dorsiflexion during stance to align the foot with the ground slope. Because of the consistent walking speed, swing knee flexion remained consistent across inclines as expected [47], [51].

Prosthetic joint kinetics at small ground slopes (±2.5 deg) are similar to level ground (Fig. 9c–f). Torque and power delivery during stance increased for inclines greater than +5.0 deg, providing a greater vertical force to the subject's center of mass. Ankle work tended to increase with ground slope (Fig. 9h), but the trend is not as obvious as the variable speed case (Fig. 7h). The total work done by the prosthesis was negative for positive slopes, possibly because the actuators were optimized for level-ground walking or because the kinematic data [47] encoded into the incline virtual constraints did not provide adequate power delivery (see Section V-B).

For a closer look at another representative subject, Fig. 10 displays the mean and variance of prosthesis kinematics and kinetics for TF03 on a 7.5 deg incline. The averaged results largely match the 7.5 deg case of subject TF02 (Fig. 9), except the ankle provided more positive work for TF03 (Fig. 10j). The ankle pushoff torque and power in Fig. 10 have similar amplitudes to the level-ground case of TF01 in Fig. 6. The inclined results in Fig. 10

exhibit slightly more variance than the level-ground case, possibly because inclined walking is a more intense activity.

V. DISCUSSION

The goal of this work was to unify the gait cycle in prosthetic leg control using a continuous sense of phase. We showed that periodic virtual constraints can be defined for any speed/slope condition using the same phase variable, which enabled multiple amputee subjects to walk in those conditions using the same fixed control gains. The phase variable accommodated different walking speeds with fixed virtual constraints, but utilizing speed-specific virtual constraints improved leg energetics. These results motivate future implementation of continuous-phase controllers within task-level finite state machines, leveraging the rich literature on speed/slope detection [52], [53] and activity mode/intent recognition [54]–[57].

A. Advantages of the Control Method

The primary clinical benefit of the continuous-phase control approach is a significant reduction in the dimension of the parameter space, which greatly reduces the configuration time for each amputee user. Current approaches that use different controllers for distinct phases of gait [4], [6]–[13] have dozens of control gains and switching rules that require hours of tuning for each user [14]. The continuous control approach eliminates all switching conditions between gait phases and uses fixed PD gains, making it less sensitive to the ambulation mode and user than existing approaches. The phase variable provides the temporal synchronization needed to walk at variable speeds even with fixed virtual constraints, but speed-matched joint kinematics provide more appropriate adjustments in prosthetic leg work. It appears that normative able-bodied joint trajectories are an adequate starting point for different amputee subjects, though better user-specific performance could possibly be achieved with minimal tuning of the reference trajectories. The four PD gains could also be quickly modified by a clinician or an automatic tuning method such as [15]–[18], [58]. Hence, the continuous-phase control approach brings powered prosthetic legs closer to plug-and-play functionality across amputee patients.

These experiments also demonstrate that the human-inspired phase variable (the thigh phase angle) effectively synchronizes the powered prosthesis with the user's gait across speeds and inclines. Because hip motion reflects the natural variability between strides (e.g., some faster than others), prosthetic joint patterns appropriately accelerated or decelerated to match and complete each stride in sync with the user (Fig. 6). The phase variable also maintained the correct timing of critical events such as ankle pushoff and swing knee flexion as conditions varied (Figs. 7 and 9), which is difficult to achieve with finite state machines. The periodic, unified virtual constraints produced very smooth, continuous joint motion within and across strides, which is also difficult to achieve when switching between finite states. One exception in the literature [19] has demonstrated similar ankle work and smoothness over variable speeds using a finite state machine based on quasi-stiffness during stance and minimum-jerk trajectories during swing.

Several qualitative observations were made during the experiments. The amputee subjects mentioned the prosthetic leg's synchronization with their intended motion. One subject mentioned relief of back pain while using the powered prosthesis compared to their passive take-home prosthesis, despite the fact that the powered leg was heavier. This feeling of relief was likely a consequence of the energy input from the powered joints, which minimized the need for hip compensations to initiate swing knee flexion and extension as required with a passive prosthetic leg [1]–[3]. The powered ankle pushoff likely helped propel the leg into swing, so the user did not notice the extra weight of the leg while walking. The amputee subjects were given a post-experiment questionnaire to provide additional feedback, and they unanimously noted the benefits of the ankle push-off at terminal stance and the aiding knee moment during swing.

B. Limitations of the Study

The primary limitation of the presented control approach is the requirement of a well-defined thigh orbit (Fig. 3) to calculate the continuous phase variable (Eq. 7). This means that the control approach works best during rhythmic walking and not during start/stop transitions. A piecewise continuous version of this control approach was recently introduced in [59] to accommodate non-rhythmic, volitional motions such as starting, stopping, and walking backwards. The piecewise phase variable is determined directly from the thigh angle (without its integral or derivative), where a ground contact sensor determines whether the thigh angle is in the top or bottom half of its orbit. The piecewise controller can work in tandem with the continuous-phase controller to accommodate both non-rhythmic and rhythmic motions [59].

Hardware limitations were more prominent at the larger inclines and faster speeds because the actuators were optimized for the torque/speed requirements of level-ground walking. Because inclined walking demands large ankle torques, the ankle motor driver intermittently disabled itself (for milliseconds at a time) when exceeding its temperature safety threshold. This behavior caused larger variances in ankle torque/power than knee torque/power in Fig. 10. Because the large reflected inertia of the highly geared knee actuator was not compensated by closed-loop torque control, the knee joint was unable to swing freely. As a result, the knee joint had difficulty keeping up with the desired swing motion at the faster walking speeds, and the subject experienced stiffer interaction with the prosthesis. These limitations will be addressed in future designs with purely rotational actuators using high-torque pancake motors, low-ratio transmissions, and high amperage drivers as in [60]. Series elastic actuators [44], [61], [62] could also make the system more compliant and provide closed-loop torque control for enforcing the virtual constraints.

The experiments in Section IV demonstrate that leg performance also depends on the reference trajectories encoded into the virtual constraints. A different able-bodied dataset was used to define the level-ground, variable-speed walking trajectories [5] than the variable-incline, normal-speed walking trajectories [47], which might explain why the work done by the prosthesis was not as favorable over inclines (Fig. 9h) as it was over speeds (Fig. 7h). Ankle work and total work were substantially higher for the level-ground condition (using data from [5]) than the incline conditions (using data from [47]) in Fig. 9h, and it is

unlikely that hardware limitations alone would be responsible for the drop in work observed at small slopes (± 2.5 deg) compared to level ground. A post-hoc analysis of the two datasets suggests that inclines affect the temporal offset between heel strike and the leftmost point of the thigh orbit, which defines 0% gait for the phase variable (Fig. 3). Hence, the phase variable may need to be shifted relative to the incline in order to achieve optimal power delivery, which is left to future work.

Because activity recognition was outside the scope of this paper, the virtual constraints were manually changed to match the speed/incline condition. The discrete set of virtual constraints that was validated in this study could be incorporated into a higher-level task state machine, for which many classification techniques exist [54]–[57]. In particular, a gait speed classifier can be implemented based on the cadence of the prosthesis, and the ground slope can be estimated by a foot-mounted IMU when the foot is flat on the ground (e.g., [52]).

VI. Conclusion

A continuous, unified-stride control approach based on a human-inspired phase variable was implemented and validated on a powered knee-ankle prosthesis, allowing three above-knee amputee subjects to walk naturally at several speed and slope conditions. This control method continuously synchronizes the prosthesis with the user's gait instead of discretely switching controllers based on switching rules, which tend to be sensitive to the user's weight and preferred gait [14]. The continuous-phase controller required no re-tuning of the control gains across the activities or users, which effectively reduced the configuration time for each amputee subject. However, clinicians could be given the ability to adjust the four control gains and/or reference trajectories to optimize clinical outcomes.

Virtual constraints could similarly be defined for stair ascent/descent using the same phase variable, because the requirement of sinusoidal hip kinematics is also satisfied during these activities [5], [63]. Task-specific virtual constraints can then be integrated with high-level intent recognition methods (e.g., [54]–[57]) to achieve seamless variable-activity control of powered prosthetic legs. It may also be possible to unify the control of prosthetic legs across tasks [47]. These future directions will improve the clinical viability of powered prosthetic legs and enable lower-limb amputees to more effectively navigate their homes and communities.

Supplementary Material

Refer to Web version on PubMed Central for supplementary material.

Acknowledgments

Villarreal holds a Graduate Fellowship from the National Council of Science and Technology (CONACYT) from Mexico.

Biographies

David Quintero (S′15) received the B.S. degree (2006) in mechanical engineering from Texas A&M University and the M.S. degree (2008) in mechanical engineering from Stanford University. He is currently pursuing a Ph.D. in Mechanical Engineering at the University of Texas at Dallas. His research is in robotics, controls, system identification, and wearable sensing for applications in rehabilitation.

Dario J. Villarreal (S′13-M′17) received the B.Eng. degree (2012) in mechatronics engineering from the Saltillo Institute of Technology and the Ph.D. degree (2017) in Biomedical Engineering at the University of Texas at Dallas.

He joined the Department of Electrical Engineering at the Southern Methodist University as an Assistant Professor in 2017. His research is in biomechatronics, robotics, systems/ controls, neuromechanics, and gait analysis with emphasis on wearable technologies such as prostheses and exoskeletons.

Daniel J. Lambert (S′15) will receive the B.S. degree (2018) in electrical engineering from the University of Texas at Dallas. He joined the Locomotor Control Systems Laboratory at The University of Texas at Dallas as an undergraduate researcher in 2014.

Susan Kapp received her B.S. degree (1979) in sociology from Texas A&M University, Prosthetic (1980) and Orthotic (1990) certificates from Northwestern University and the M.Ed. degree (2005) from the University of Texas.

She joined the Department of Rehabilitation Medicine at the University of Washington (UW) as a lecturer in 2017. Prior to joining UW, she was an Associate Professor and the director of the Prosthetics-Orthotics Program at the University of Texas Southwestern Medical Center in Dallas, TX. Her research interests relate to prosthetic socket volume and pressure as well as prosthetic component selection.

Robert D. Gregg (S´08-M´10-SM´16) received the B.S. degree (2006) in electrical engineering and computer sciences from the University of California, Berkeley and the M.S. (2007) and Ph.D. (2010) degrees in electrical and computer engineering from the University of Illinois at Urbana-Champaign.

He joined the Departments of Bioengineering and Mechanical Engineering at the University of Texas at Dallas (UTD) as an Assistant Professor in 2013. Prior to joining UTD, he was a Research Scientist at the Rehabilitation Institute of Chicago and a Postdoctoral Fellow at Northwestern University. His research is in the control of bipedal locomotion with applications to autonomous and wearable robots.

References

1. Smith D, Michael J, , Bowker J, editorsAtlas of Amputations and Limb Deficiencies: Surgical, Prosthetic, and Rehabilitation Principles Rosemont IL: American Academy of Orthopaedic Surgeons; 2004

2. Sanderson DJ, Martin PE. Lower extremity kinematic and kinetic adaptations in unilateral below-knee amputees during walking. Gait & Posture. 1997; 6(2):126–136.

3. Rabuffetti M, Recalcati M, Ferrarin M. Trans-femoral amputee gait: Socket–pelvis constraints and compensation strategies. Prosthet Orthot Int. 2005; 29(2):183–192. [PubMed: 16281727]

4. Tucker MR, Olivier J, Pagel A, Bleuler H, Bouri M, Lambercy O, del R Millán J, Riener R, Vallery H, Gassert R. Control strategies for active lower extremity prosthetics and orthotics: a review. J Neuroeng Rehabil. 2015; 12(1)

5. Winter D. Biomechanics and Motor Control of Human Gait 2nd. Ontario: University of Waterloo Press; 1991

6. Sup F, Bohara A, Goldfarb M. Design and control of a powered transfemoral prosthesis. Int J Robot Res. 2008; 27(2):263–273.

7. Au SK, Herr H. Powered ankle-foot prosthesis. IEEE Robot Automat Mag. 2008; 15(3):52–59.

8. Sup F, Varol HA, Mitchell J, Withrow TJ, Goldfarb M. Preliminary evaluations of a self-contained anthropomorphic transfemoral prosthesis. IEEE/ASME Trans Mechatronics. 2009; 14(6):667–676. [PubMed: 20054424]

9. Sup F, Varol HA, Goldfarb M. Upslope walking with a powered knee and ankle prosthesis: initial results with an amputee subject. IEEE Trans Neural Sys Rehab Eng. 2011; 19(1):71–78.

10. Lawson BE, Mitchell J, Truex D, Shultz A, Ledoux E, Goldfarb M. A robotic leg prosthesis: Design, control, and implementation. IEEE Robot Autom Mag. 2014; 21(4):70–81.

11. Eilenberg MF, Geyer H, Herr H. Control of a powered ankle-foot prosthesis based on a neuromuscular model. IEEE Trans Neural Sys Rehab Eng. 2010; 18(2):164–173.

12. Thatte N, Geyer H. Toward balance recovery with leg prostheses using neuromuscular model control. IEEE Trans Biomed Eng. 2016; 63(5):904–913. [PubMed: 26315935]

13. Lawson B, Varol H, Huff A, Erdemir E, Goldfarb M. Control of stair ascent and descent with a powered transfemoral prosthesis. IEEE Trans Neural Sys Rehab Eng. 2013; 21(3):466–473.

14. Simon AM, Ingraham KA, Fey NP, Finucane SB, Lipschutz RD, Young AJ, Hargrove LJ. Configuring a powered knee and ankle prosthesis for transfemoral amputees within five specific ambulation modes. PLoS ONE. 2014; 9(6):e99387. [PubMed: 24914674]

15. Aghasadeghi N, , Zhao H, , Hargrove L, , Ames A, , Perreault E, , Bretl T. Learning impedance controller parameters for lower-limb prostheses. IEEE International Conference on Intelligent Robots and Systems IEEE; 2013 42684274

16. Koller JR, , Gates DH, , Ferris DP, , Remy CD. Body-in-the-loop optimization of assistive robotic devices: A validation study. Robotics: Science and Systems Conference; 2016

17. Zhang J, Fiers P, Witte KA, Jackson RW, Poggensee KL, Atkeson CG, Collins SH. Human-in-the-loop optimization of exoskeleton assistance during walking. Science. 2017; 356(6344):1280–1284. [PubMed: 28642437]

18. Huang H, Crouch DL, Liu M, Sawicki GS, Wang D. A cyber expert system for auto-tuning powered prosthesis impedance control parameters. Annals Biomed Eng. 2016; 44(5):1613–1624.

19. Lenzi T, Hargrove L, Sensinger J. Speed-adaptation mechanism: Robotic prostheses can actively regulate joint torque. IEEE Robot Automat Mag. 2014; 21(4):94–107.

20. Westervelt ER, , Grizzle JW, , Chevallereau C, , Choi JH, , Morris B. Feedback Control of Dynamic Bipedal Robot Locomotion Boca Raton Florida: CRC Press; 2007

21. Grizzle JW, Abba G, Plestan F. Asymptotically stable walking for biped robots: analysis via systems with impulse effects. IEEE Trans Automat Contr. 2001; 46(3):513–513.

22. Sreenath K, Park H-W, Poulakakis I, Grizzle JW. A compliant hybrid zero dynamics controller for stable, efficient and fast bipedal walking on MABEL. Int J Robot Res. 2011; 30(9):1170–1193.

23. Ramezani A, Hurst J, Hamed K, Grizzle J. Performance analysis and feedback control of ATRIAS, a three-dimensional bipedal robot. ASME J Dyn Sys Meas Control. 2013; 136(2):021012.

24. Buss B, Ramezani A, Hamed K, Griffin B, Galloway K, Grizzle J. Preliminary walking experiments with underactuated 3d bipedal robot MARLO. IEEE Int Conf Intelli Robots Sys. 2014:2529–2536.

25. Hamed KA, , Buss BG, , Grizzle JW. Continuous-time controllers for stabilizing periodic orbits of hybrid systems: Application to an underactuated 3D bipedal robot. IEEE Conf Decis Control; 2014 15071513

26. Martin AE, Post DC, Schmiedeler JP. Design and experimental implementation of a hybrid zero dynamics-based controller for planar bipeds with curved feet. Int J Robot Res. Jun.2014 33(7): 988–1005.

27. Veer S, , Motahar MS, , Poulakakis I. On the adaptation of dynamic walking to persistent external forcing using hybrid zero dynamics control. IEEE Int Conf Intelli Robots Sys; 2015 9971003

28. Kong FH, , Boudali AM, , Manchester IR. Phase-indexed ilc for control of underactuated walking robots; IEEE Conf Control Applicat; 2015 14671472

29. Villarreal DJ, Poonawala H, Gregg RD. A robust parameterization of human joint patterns across phase-shifting perturbations. IEEE Trans Neural Sys Rehab Eng. 2017; 25(3):265–278.

30. Villarreal D, Gregg R. Unified phase variables of relative degree two for human locomotion. IEEE Int Conf Eng Med Biol Soc. 2016:6262–6267.

31. Lenggenhager B, Arnold CA, Giummarra MJ. Phantom limbs: pain, embodiment, and scientific advances in integrative therapies. Wiley Interdisciplinary Reviews: Cogn Sci. 2014; 5(2):221–231.

32. Gregg RD, Lenzi T, Hargrove LJ, Sensinger JW. Virtual constraint control of a powered prosthetic leg: From simulation to experiments with transfemoral amputees. IEEE Trans Robot. 2014; 30(6): 1455–1471. [PubMed: 25558185]

33. Martin AE, , Gregg RD. Hybrid invariance and stability of a feedback linearizing controller for powered prostheses. Amer Contr Conf; Chicago, IL. 2015 46704676

34. Martin AE, Gregg RD. Stable, robust hybrid zero dynamics control of powered lower-limb prostheses. IEEE Trans Automat Contr. 2017; 62(8):3930–3942. [PubMed: 29276305]

35. Zhao H, Horn J, Reher J, Paredes V, Ames AD. First steps toward translating robotic walking to prostheses: a nonlinear optimization based control approach. Auton Robots. 2017; 41(3):725–742.

36. Holgate MA, , Sugar TG, , Bohler A. A novel control algorithm for wearable robotics using phase plane invariants. IEEE Int Conf Robot Automat; 2009 38453850

37. Kerestes J, , Sugar TG, , Holgate M. Adding and subtracting energy to body motion: Phase oscillator. ASME Int Design Eng Tech Conf & Comp and Info in Eng Conf; 2014 V05AT08A004

38. Lenzi T, Carrozza MC, Agrawal SK. Powered hip exoskeletons can reduce the user's hip and ankle muscle activations during walking. IEEE Trans Neural Sys Rehab Eng. 2013; 21(6):938–948.

39. Isidori A. Nonlinear Control Systems 3rd. London, England: Springer; 1995

40. Quintero D, Martin AE, Gregg RD. Toward unified control of a powered prosthetic leg: A simulation study. IEEE Trans Control Syst Technol. 2018; 26(1):305–312. [PubMed: 29403259]

41. Quintero D, , Villarreal DJ, , Gregg RD. Preliminary experiments with a unified controller for a powered knee-ankle prosthetic leg across walking speeds. IEEE Int Conf Intelli Robots Sys; 2016 54275433

42. Pieringer DS, , Grimmer M, , Russold MF, , Riener R. Review of the actuators of active knee prostheses and their target design outputs for activities of daily living. IEEE Int Conf Rehab Robotics; 2017 12461253

43. Grey MJ, Nielsen JB, Mazzaro N, Sinkjær T. Positive force feedback in human walking. The Journal of physiology. 2007; 581(1):99–105. [PubMed: 17331984]

44. Grimmer M, , Eslamy M, , Gliech S, , Seyfarth A. A comparison of parallel- and series elastic elements in an actuator for mimicking human ankle joint in walking and running. IEEE Int Conf Robotics & Automation; 2012 24632470

45. Jaritz A, Spong MW. An experimental comparison of robust control algorithms on a direct drive manipulator. IEEE Trans Control Systems Technology. 1996; 4(6):627–640.

46. Oppenheim AV, , Schafer RW. Discrete-Time Signal Processing 3rd. New York City, NY: Pearson; 2013

47. Embry KR, , Villarreal DJ, , Gregg RD. A unified parameterization of human gait across ambulation modes. IEEE Int Conf Eng Med Biol Soc; 2016 21792183

48. Rossignol S, Dubuc R, Gossard J-P. Dynamic sensorimotor interactions in locomotion. Physiol Rev. 2006; 86(1):89–154. [PubMed: 16371596]

49. Jolliffe I. Principal Component Analysis Wiley Online Library 2002

50. DeVita P, Helseth J, Hortobagyi T. Muscles do more positive than negative work in human locomotion. J Exp Biol. 2007; 210(19):3361–3373. [PubMed: 17872990]

51. McIntosh AS, Beatty KT, Dwan LN, Vickers DR. Gait dynamics on an inclined walkway. J Biomech. 2006; 39(13):2491–2502. [PubMed: 16169000]

52. Sabatini AM, Martelloni C, Scapellato S, Cavallo F. Assessment of walking features from foot inertial sensing. IEEE Trans Biomed Eng. 2005; 52(3):486–494. [PubMed: 15759579]

53. Quintero D, , Lambert D, , Villarreal D, , Gregg R. Real-time continuous gait phase and speed estimation from a single sensor. IEEE Conf Contr Technol Applicat; 2017847852

54. Preece SJ, Goulermas JY, Kenney LP, Howard D, Meijer K, Crompton R. Activity identification using body-mounted sensors: a review of classification techniques. Physiological Measurement. 2009; 30(4):R1–R33. [PubMed: 19342767]

55. Huang H, Kuiken TA, Lipschutz RD. A strategy for identifying locomotion modes using surface electromyography. IEEE Trans Biomed Eng. 2009; 56(1):65–73. [PubMed: 19224720]

56. Varol H, Sup F, Goldfarb M. Multiclass real-time intent recognition of a powered lower limb prosthesis. IEEE Trans Biomed Eng. 2010; 57(3):542–551. [PubMed: 19846361]

57. Young AJ, Simon AM, Fey NP, Hargrove LJ. Intent recognition in a powered lower limb prosthesis using time history information. Annals Biomed Eng. 2014; 42(3):631–641.

58. Kumar S, , Mohammadi A, , Gans N, , Gregg R. Automatic tuning of virtual constraint-based control algorithms for powered knee-ankle prostheses. IEEE Conf Contr Technol Applicat; 2017812818

59. Villarreal DJ, Quintero D, Gregg RD. Piecewise and unified phase variables in the control of a powered prosthetic leg. IEEE Int Conf Rehab Robot. 2017:1425–1430.

60. Zhu H, Doan J, Stence C, Lv G, Elery T, Gregg R. Design and validation of a torque dense, highly backdrivable powered knee-ankle orthosis. IEEE Int Conf Robot Autom. 2017:504–510. [PubMed: 29057142]

61. Rouse EJ, Mooney LM, Herr HM. Clutchable series-elastic actuator: Implications for prosthetic knee design. Int J Robotics Research. 2014; 33(13):1611–1625.

62. Pfeifer S, Pagel A, Riener R, Vallery H. Actuator with angle-dependent elasticity for biomimetic transfemoral prostheses. IEEE/ASME Trans Mechatronics. 2015; 20(3):1384–1394.

63. Villarreal DJ, , Gregg RD. A survey of phase variable candidates of human locomotion. IEEE Int Conf Eng Med Biol Soc; Chicago, IL. 2014 40174021
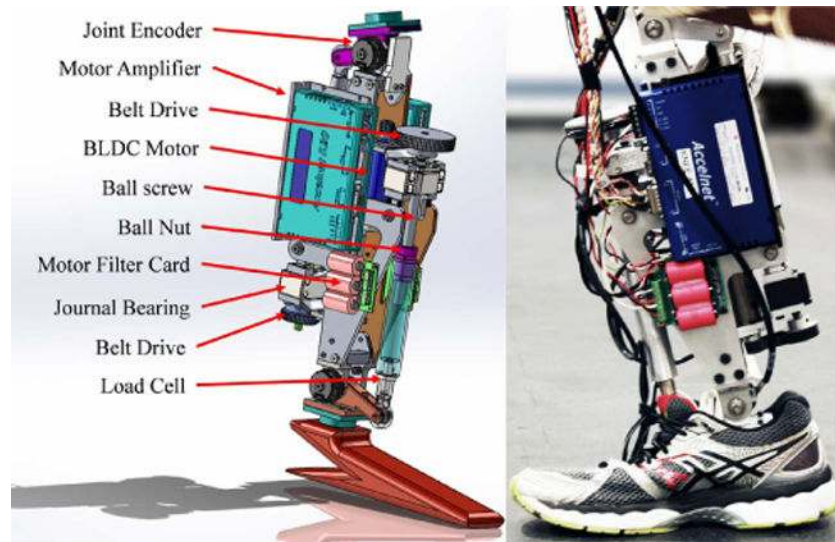
Fig. 1.
The UT Dallas powered knee-ankle prosthesis: CAD rendering and key components (left) and manufactured version (right). A timing belt connects each motor to a linear ball screw, which converts rotary motion to translational motion that drives a lever arm to produce a joint torque.
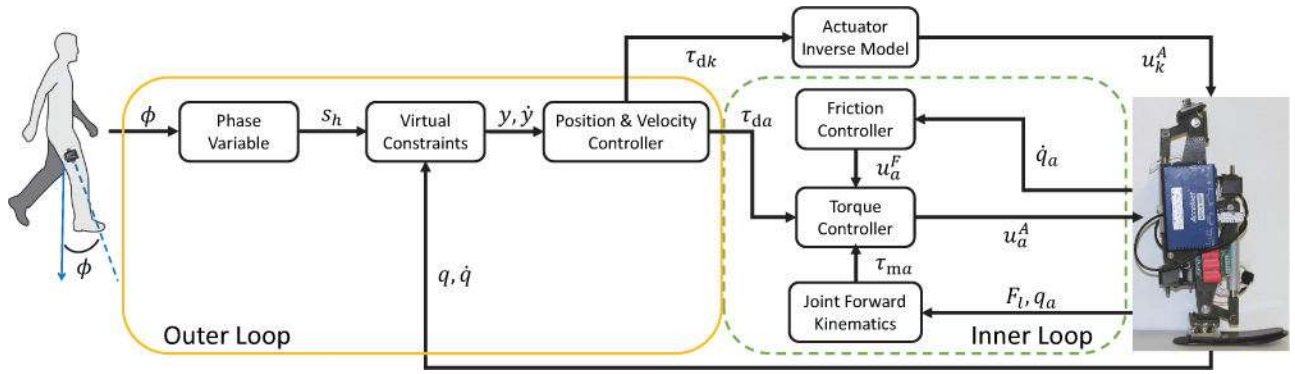
Fig. 2.
The control architecture for the prosthesis comprises an outer and inner loop. The outer loop computes the desired joint torques (Eq. 2) needed to enforce the virtual constraints (Eq. 5) based on the mechanical phase variable (Eq. 7). The desired knee torque $\tau_{\mathrm{d}k}$ is converted to current commands for the knee motor driver (u_k^A) using an inverse model of the knee actuator. The current commands for the ankle motor driver (u_a^A) are computed by an inner loop (Eq. 10) that provides closed-loop torque control with a friction compensator.
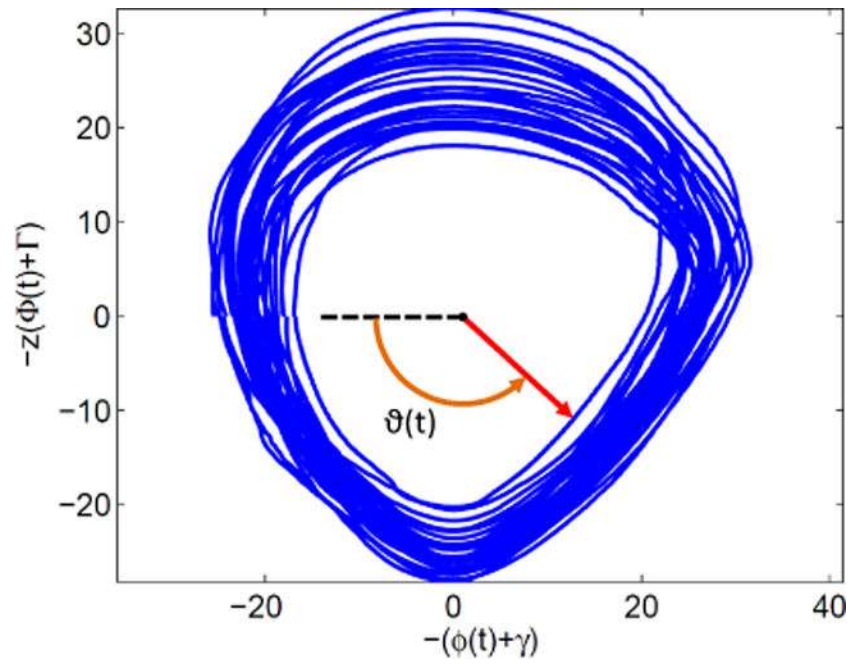
Fig. 3.
Phase plane of the thigh angle $\phi(t)$ vs. its integral $\Phi(t)$ during prosthetic leg experiments (Section IV). The phase plane has been scaled by z and shifted by (γ, Γ) to achieve a circular orbit across the stride, which improves the linearity of the phase variable $\vartheta(t)$.
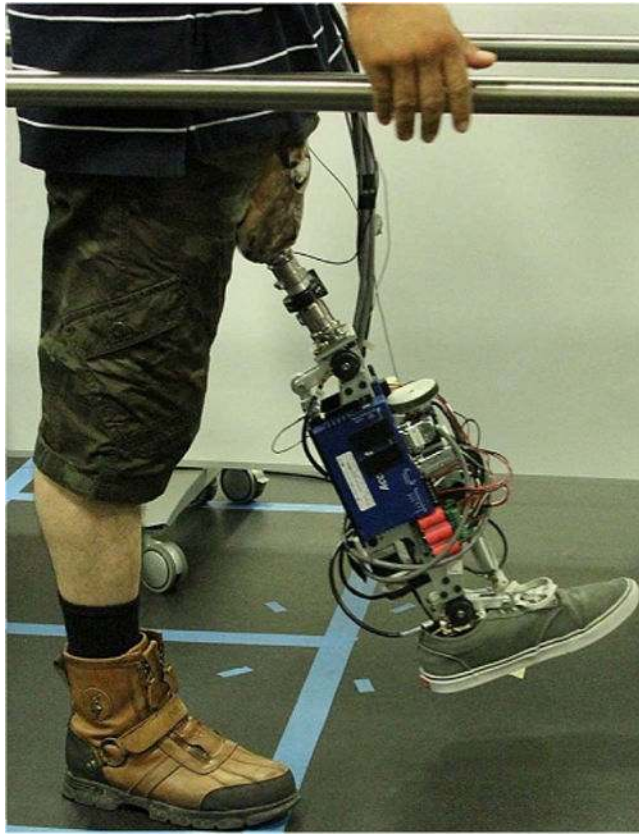
Fig. 4.
Photo of transfemoral amputee subject wearing the powered knee-ankle prosthesis. The IMU sensor is mounted on the pylon between the residual limb socket and the prosthetic knee joint (in the sagittal plane).
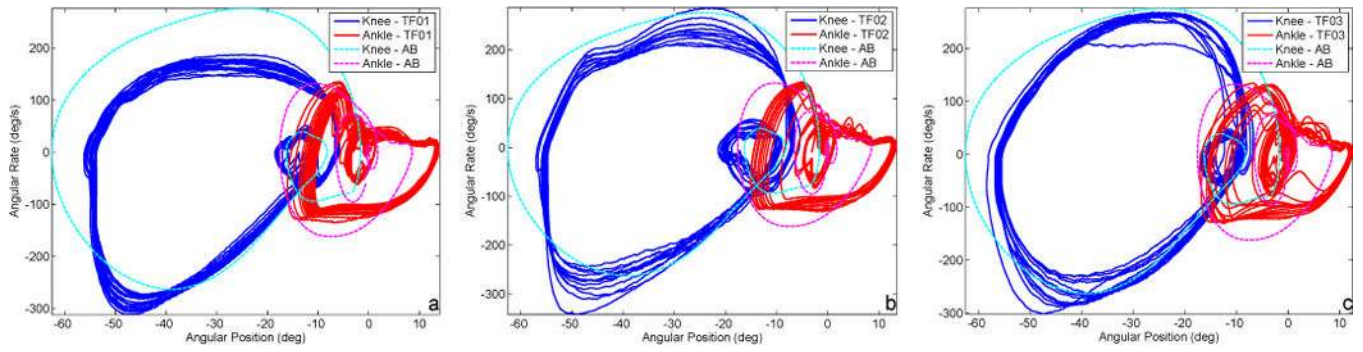
Fig. 5.
Phase portrait of the prosthetic leg (measured joint angular positions vs. velocities) over 20 consecutive strides of steady-state, level-ground walking at the comfortable speed (about 2.0 mph) for amputee subjects TF01 (left), TF02 (center), and TF03 (right), compared with averaged able-bodied data (AB) [5]. Note that the prosthetic joints follow similar orbits to the able-bodied data.
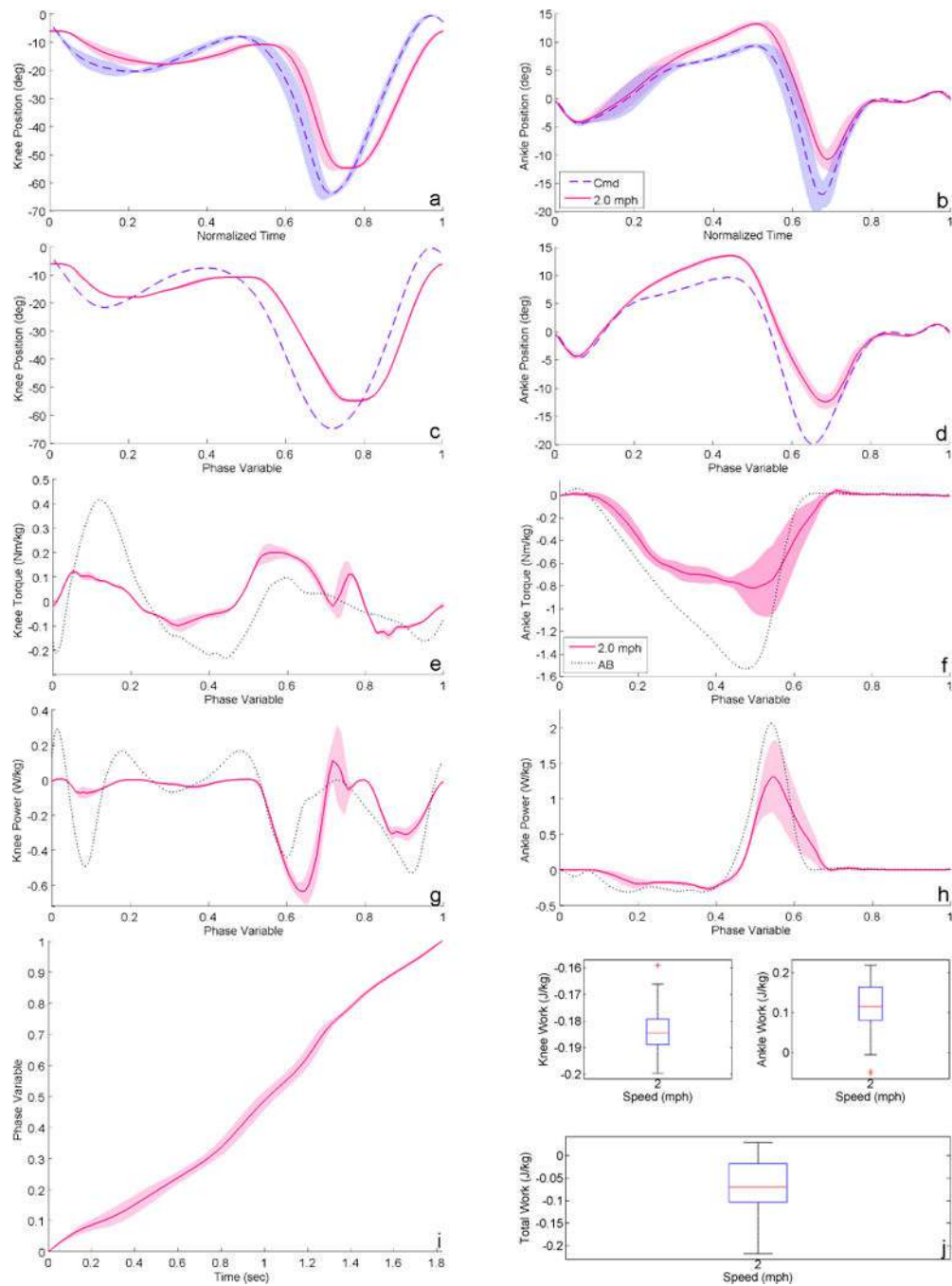
Fig. 6.
Powered prosthesis joint kinematics/kinetics for TF01 level-ground walking at 2.0 mph, averaged over 20 consecutive strides with ±1 standard deviation shown by shaded regions. The commanded (Cmd) and measured (2.0 mph) joint angles are shown over normalized time (a–b) and over the phase variable (c–d). The estimated joint torques (e–f) and powers (g–h) are normalized by subject mass and compared with averaged able-bodied data (AB) over the phase variable [5]. The knee torque is estimated with the measured motor current and the knee actuator model, and the ankle torque is estimated with the measured linear

force and ankle kinematic model (Fig. 2). The phase variable over time (i) is strictly monotonic and nearly linear, where the most variance occurs during early and mid stance. Box plots of mechanical work per stride (j) show the median (red line), 25th percentile (bottom of box), 75th percentile (top of box), distribution bounds (black whiskers), and outliers (red plus markers). Ankle work is positive, knee work is negative, and total work is near zero as expected from able-bodied walking [5].
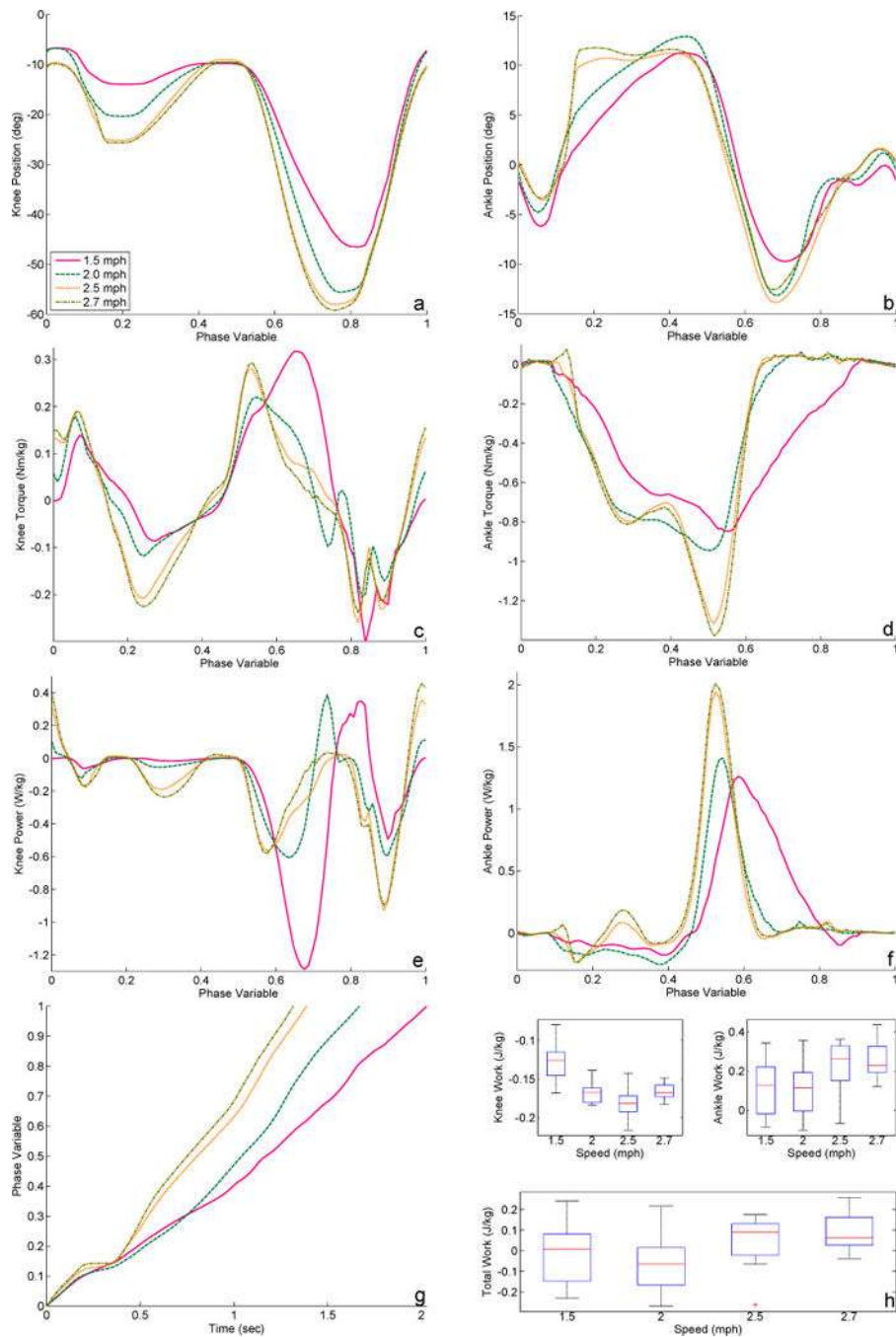
Fig. 7.
Powered prosthesis joint kinematics/kinetics for TF02 level-ground walking at multiple speeds with slow, normal, and fast kinematics, averaged over 15–20 consecutive strides. The measured joint angles over phase (a–b) demonstrate that faster speeds produce a larger range of motion. The estimated joint torques (c–d) and powers (e–f) are normalized by subject mass and plotted over phase, demonstrating more torque and power at faster speeds. The phase variable over time (g) is monotonic with a steeper slope (i.e., shorter time duration) for faster speeds. Box plots of mechanical work per stride (h) show the median (red line),

25th percentile (bottom of box), 75th percentile (top of box), distribution bounds (black whiskers), and outliers (red plus markers) for each speed condition. Ankle work and total work increase with walking speed as expected [5].
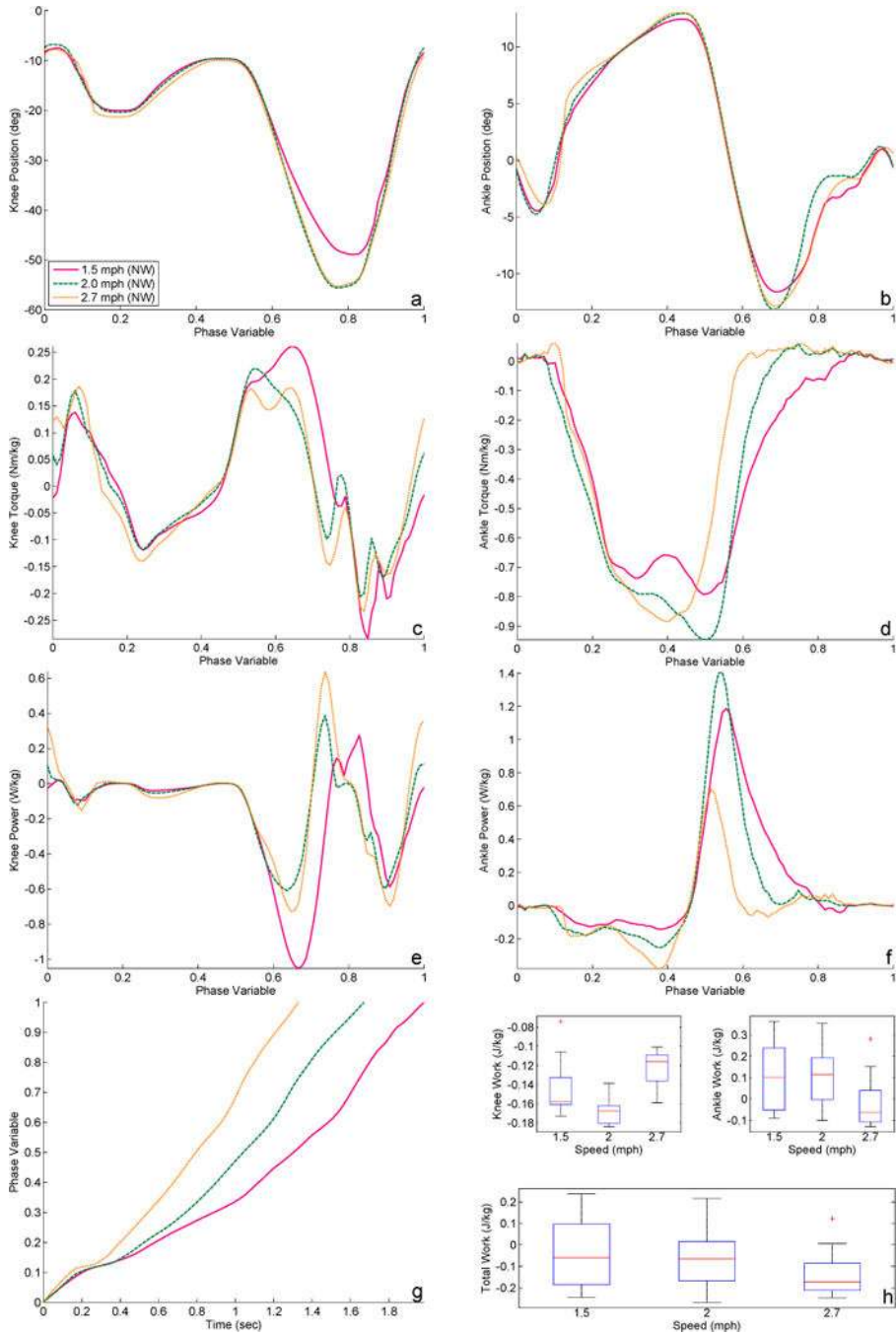
Fig. 8.
Powered prosthesis joint kinematics/kinetics for TF02 level-ground walking at multiple speeds with fixed normal-speed kinematics, averaged over 15–20 consecutive strides. The measured joint angles (a–b), normalized joint torques (c–d), and normalized joint powers (e–f) are more appropriate for slow and normal speeds than the fastest speed. The phase variable over time (g) adapts appropriately with all speeds, having a steeper slope (i.e., shorter time duration) for faster speeds. Box plots of mechanical work per stride (h) show the median (red line), 25th percentile (bottom of box), 75th percentile (top of box),

distribution bounds (black whiskers), and outliers (red plus markers) for each speed condition. Ankle work and total work are appropriate for slow and normal walking but insufficient for the fastest speed [5].
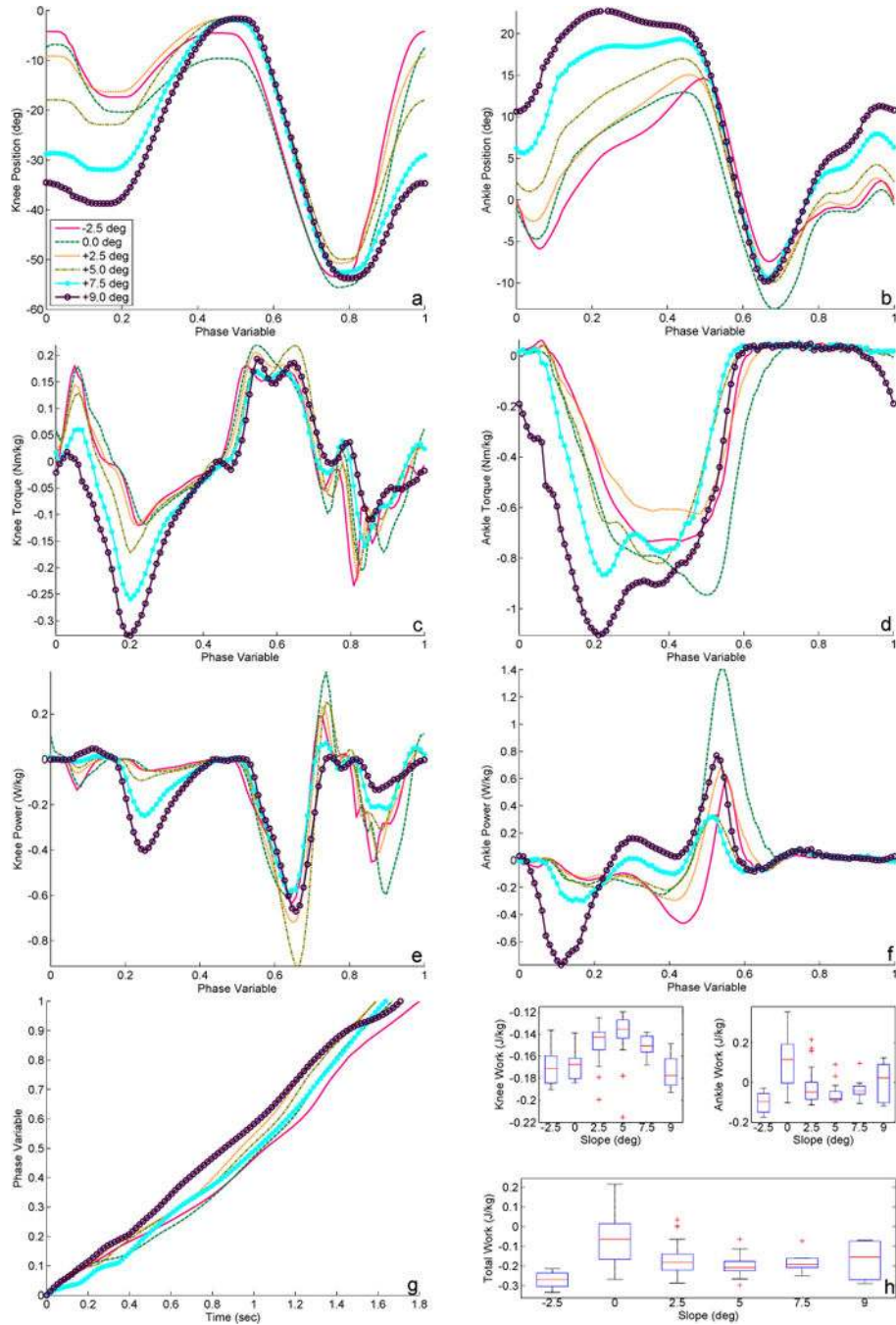
Fig. 9.
Powered prosthesis joint kinematics/kinetics for TF02 walking on multiple ground slopes at 2.0 mph with slope-specific kinematics, averaged over 10–20 consecutive strides. The measured joint angles over phase (a–b) exhibit more stance ankle dorsiflexion and stance knee flexion/extension for steeper inclines. The estimated joint torques (c–d) and powers (e–f) are normalized by subject mass and plotted over phase. The phase variable over time (g) has a consistent, linear trajectory across ground slopes (i.e., similar time durations). Box plots of mechanical work per stride (h) show the median (red line), 25th percentile (bottom

of box), 75th percentile (top of box), distribution bounds (black whiskers), and outliers (red plus markers) for each slope condition.
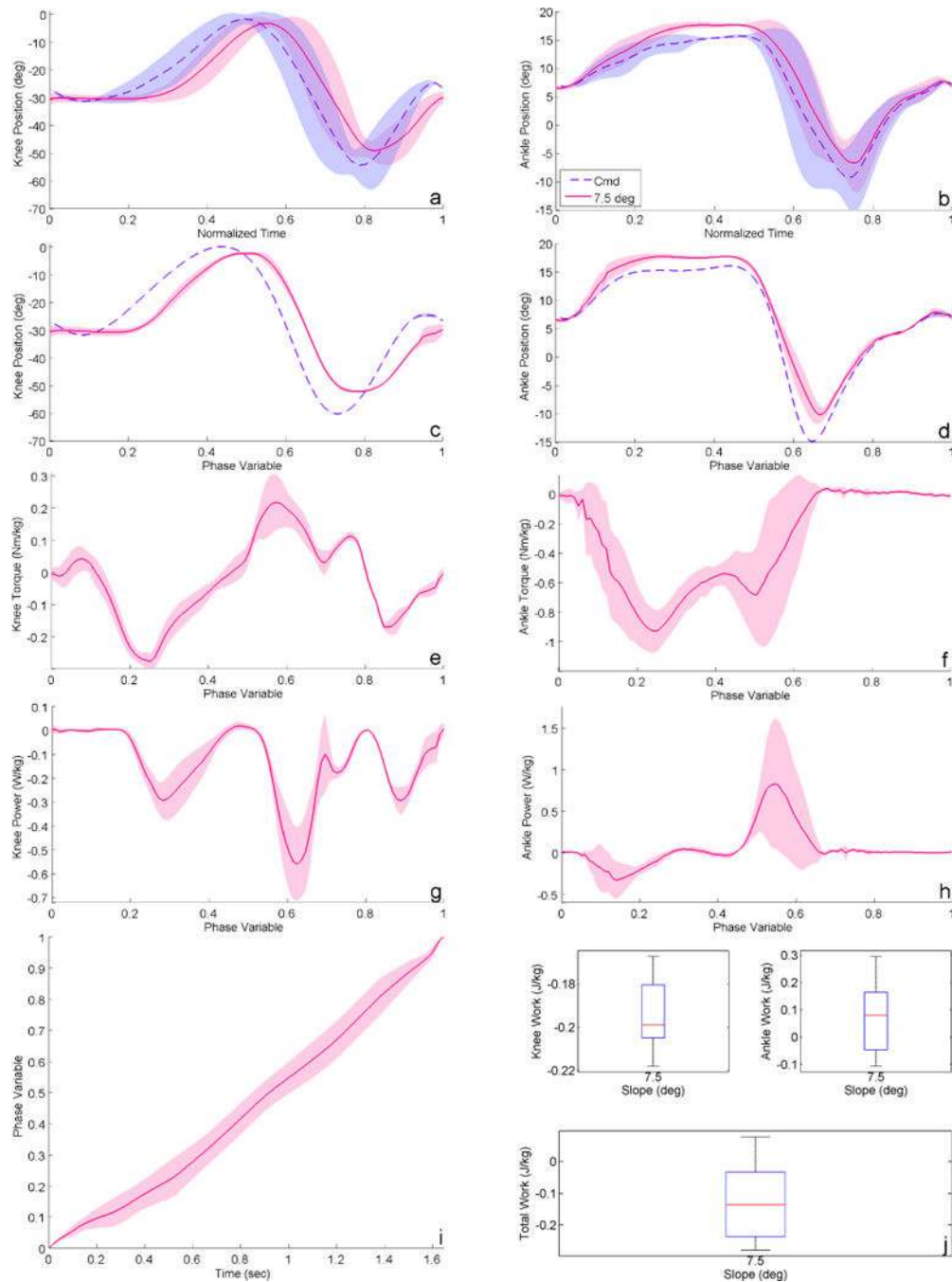
Fig. 10.
Powered prosthesis joint kinematics/kinetics for TF03 walking on 7.5 deg incline at 2.0 mph, averaged over 9 consecutive strides with ±1 standard deviation shown by shaded regions. The commanded (Cmd) and measured (7.5 deg) joint angles are shown over normalized time (a–b) and over the phase variable (c–d). The commanded signals have some variance at the end of the stride due to the use of a rate limiter as a safety feature. The estimated joint torques (e–f) and powers (g–h) are normalized by subject mass and shown over the phase variable. The phase variable over time (i) is strictly monotonic and nearly

linear. Box plots of mechanical work per stride (j) show the median (red line), 25th percentile (bottom of box), 75th percentile (top of box), distribution bounds (black whiskers), and outliers (red plus markers).

TABLE I

Characteristics of Transfemoral Amputee Subjects

Subject	Gender	Height (m)	Weight (kg)	Age (yrs)	Post-Amputation Time (yrs)	Amputated Side
TF01	Male	1.702	87.1	34	18	Left
TF02	Male	1.69	65.8	29	20	Right
TF03	Male	1.78	70.6	37	7	Left

TABLE II

Ranges of Activities Performed by Transfemoral Amputee Subjects

Subject	Min Speed (mph)	Max Speed (mph)	Min Slope (deg)	Max Slope (deg)
TF01	1.5	2	−2.5	7.5
TF02	1.5	2.7	−2.5	9
TF03	1.5	2.7	−2.5	7.5